BRAIN CONNECTIVITY
Volume 7, Number 6, 2017

DOI: 10.1089/brain.2016.0477

Fine-Grained Parcellation of Brain Connectivity Improves Differentiation of States of Consciousness During Graded Propofol Sedation

Xiaolin Liu,[1] Kathryn K. Lauer,[2] B. Douglas Ward,[3] Christopher J. Roberts,[2] Suyan Liu,[2] Suneeta Gollapudy,[2] Robert Rohloff,[4] William Gross,[2] Zhan Xu,[3] Guangyu Chen,[3] Jeffrey R. Binder,[4] Shi-Jiang Li,[3] and Anthony G. Hudetz[5]

Abstract

Conscious perception relies on interactions between spatially and functionally distinct modules of the brain at various spatiotemporal scales. These interactions are altered by anesthesia, an intervention that leads to fading consciousness. Relatively little is known about brain functional connectivity and its anesthetic modulation at a fine spatial scale. Here, we used functional imaging to examine propofol-induced changes in functional connectivity in brain networks defined at a fine-grained parcellation based on a combination of anatomical and functional features. Fifteen healthy volunteers underwent resting-state functional imaging in wakeful baseline, mild sedation, deep sedation, and recovery of consciousness. Compared with wakeful baseline, propofol produced widespread, dose-dependent functional connectivity changes that scaled with the extent to which consciousness was altered. The dominant changes in connectivity were associated with the frontal lobes. By examining node pairs that demonstrated a trend of functional connectivity change between wakefulness and deep sedation, quadratic discriminant analysis differentiated the states of consciousness in individual participants more accurately at a fine-grained parcellation (e.g., 2000 nodes) than at a coarse-grained parcellation (e.g., 116 anatomical nodes). Our study suggests that defining brain networks at a high granularity may provide a superior imaging-based distinction of the graded effect of anesthesia on consciousness.

Keywords: brain parcellation; loss of consciousness; propofol sedation; resting-state fMRI; state classification

Introduction

Consciousness has been a target of scientific inquiry in anesthetized subjects, patients in unresponsive wakefulness, and various neuropsychological conditions. Consciousness is best defined as a subjective experience, which implies its phenomenal nature (Chalmers, 1998). In clinical sciences, the presence of consciousness is generally defined by the preservation of purposeful behavioral responsiveness, although it may also be implied by a covert volitional response (Monti et al., 2010). In this work, we adopt the clinical behavioral definition that a purposeful response implies the subject's ability to consciously access information, not withstanding that the converse does not negate the possibility of phenomenal experience.

Current theories postulate that the neuronal mechanism of consciousness involves the functional interaction of brain regions in a global workspace that allows the integration of information processed by different modalities (Baars, 2002, 2005; Dehaene et al., 2003; Tononi, 2012). General anesthesia may suppress consciousness by disrupting information integration (Alkire et al., 2008), essentially ''unbinding'' the pieces of information processed by various components of the global workspace (Mashour, 2013). This model implies that an understanding of the mechanisms of anesthetic suppression of consciousness requires an analysis of functional connections across the association networks of the entire brain.

Mapping the brain as a connected network requires the subdivision (parcellation) of major brain regions into smaller, structurally, and functionally connected regions, which are also called network nodes (de Reus and van den Heuvel, 2013). The current imaging-based brain parcellation approaches are based on predefined anatomical templates (Fischl et al., 2004; Tzourio-Mazoyer et al., 2002), randomly generated

Departments of [1]Radiology, [2]Anesthesiology, [3]Biophysics, and [4]Neurology, Medical College of Wisconsin, Milwaukee, Wisconsin.
[5]Department of Anesthesiology and Center for Consciousness Science, University of Michigan, Ann Arbor, Michigan.

templates (van den Heuvel and Sporns, 2011), selected putative functional areas (Power et al., 2011), and recently, multimodal gradient-based areal maps (Glasser et al., 2016). Evidence also indicates that defining brain networks at a higher granularity of parcellation allows a more prominent display of topological features of the brain (Hayasaka and Laurienti, 2010; Zalesky et al., 2010). In one of our former studies, the granularity of parcellation of brain networks was increased by dividing each anatomical region into smaller subregions based on voxel-wise functional connectivity (Liu et al., 2014). This parcellation scheme allowed us to detect whether a power-law node-degree distribution emerged in individual vegetative-state patients in comparison to healthy individuals in a state of unconsciousness during anesthetic sedation. However, such a detection capability was not possible with a coarse-grained anatomical template alone.

Former neuroimaging studies of the effects of anesthesia on consciousness identified diverse changes in brain functional connectivity, including spatiotemporal configuration (Schroter et al., 2012), global and local information processing (Monti et al., 2013), functional integration (Schrouff et al., 2011), breakdown of modular networks (Boveroux et al., 2010; Godwin et al., 2015), departure from criticality (Tagliazucchi et al., 2016), temporal variability (Huang et al., 2016), as well as various cortical and subcortical networks (Hudetz, 2012). We propose that a reason for the disparate results may be methodological due to the varied spatial granularity at which functional connectivity was examined. Also, most studies to date reported group average results, ignoring potentially important subject-specific changes. In some instances, voxel-based measures of intrinsic connectivity were used in anesthetized subjects (Martuzzi et al., 2010) and in patients with neurological and psychiatric disorders (Scheinost et al., 2012), which yield the highest granularity of blood-oxygen level dependent (BOLD) signal-based connectivity.

The goal of this study was to determine the benefit of defining brain networks by using a fine-grained parcellation up to 2000 network nodes in terms of differentiating states of consciousness as modulated by the anesthetic agent propofol. Functional imaging was performed in four states: wakeful baseline, light sedation, deep sedation, and recovery. Brain parcellation was based on the combination of anatomical and functional features (Liu et al., 2014). We then used a quadratic discriminant analysis to differentiate the four states of consciousness in individual study participants based on the extracted features of functional connectivity changes. We anticipated that a fine-grained functional parcellation would enable better differentiation of anesthetic sedation level-dependent states of consciousness in individual participants than that obtained with a coarse-grained parcellation.

Materials and Methods

The experimental protocol was approved by the Institutional Review Board of the Medical College of Wisconsin (MCW).

Study participants

Fifteen healthy volunteers aged 19–35 years (nine men and six women, mean age 26.7 years, standard deviation 4.8, body mass index < 25) provided written informed consent to participate in this study. Participants were native English speakers recruited from MCW communities with no history of neurological or psychiatric conditions.

Propofol administration

The anesthetic agent, propofol, was administered with a bolus dose followed by a target-controlled continuous infusion (STANPUMP). The pharmacokinetics and pharmacodynamics of propofol have been described in detail and mathematically modeled (Shafer et al., 1988). Propofol is a favored choice for the study because it is a fast-acting drug whose effect-site concentration can be predicted and controlled by controlled infusion. We targeted a plasma concentration of 1 μg/ml for light sedation and 2 μg/ml for deep sedation. The Observer's Assessment of Alertness and Sedation (OAAS) score was used to determine the participants' behavioral responsiveness. The OAAS is defined on a 6-point scale, as follows: 5, responds readily to name spoken in normal tone; 4, lethargic response to name spoken in normal tone; 3, responds only after name is called loudly and/or repeatedly; 2, responds only after mild prodding or shaking; 1, responds only after painful trapezius squeeze; and 0, does not respond to painful trapezius squeeze. The lower dose was intended to achieve an OAAS score of 3 or 4, and the higher dose was chosen to achieve an OAAS score of 1 or 2. The latter was defined as an unconscious state. To test behavioral responsiveness with the OAAS score, the anesthesiologist entered the scanner room and performed the defined assessment procedures at the bedside of the scanner before the next scan after the propofol reached a predicted target concentration.

Resting-state imaging acquisition

Resting-state structural and functional MRI data were acquired by using a whole-body 3T Signa GE scanner (GE Healthcare, Waukesha, Wisconsin) with a standard 32-channel transmit-receive head coil. Functional imaging data were acquired during each of four 15-minute scans in wakefulness, light sedation, deep sedation, and recovery, respectively (Fig. 1A), with repetition time, 2 s; total volumes, 450; echo time, 25 ms; slice thickness, 3.5 mm; in-plane resolution, 3.5×3.5 mm; number of slices, 41; flip angle, 77°; field of view, 22.4 cm; and matrix size, 64×64. High-resolution three-dimensional spoiled gradient-recalled echo (SPGR) axial images were acquired before functional scans with TE/TR/TI, 3.2/8.2/450 ms; slice thickness, 1 mm; 150 slices; flip angle, 12°; field of view, 24 cm; and matrix size, 256×256. Cardiac and respiratory activities were recorded.

Imaging data preprocessing

Imaging data preprocessing was conducted by using a combination of Analysis of Functional NeuroImages (AFNI),[1] Statistical Parametric Mapping (SPM),[2] FMRIB Software Library (FSL),[3] and Matlab software (The MathWorks, Natick, MA). Raw functional images first underwent retrospective correction of physiological motion effects by cardiac and respiratory activities (*3dretroicor* in AFNI). The first five data points were discarded to reduce the initial

[1]http://afni.nimh.nih.gov/afni
[2]www.fil.ion.ucl.ac.uk/spm
[3]www.fmrib.ox.ac.uk/fsl

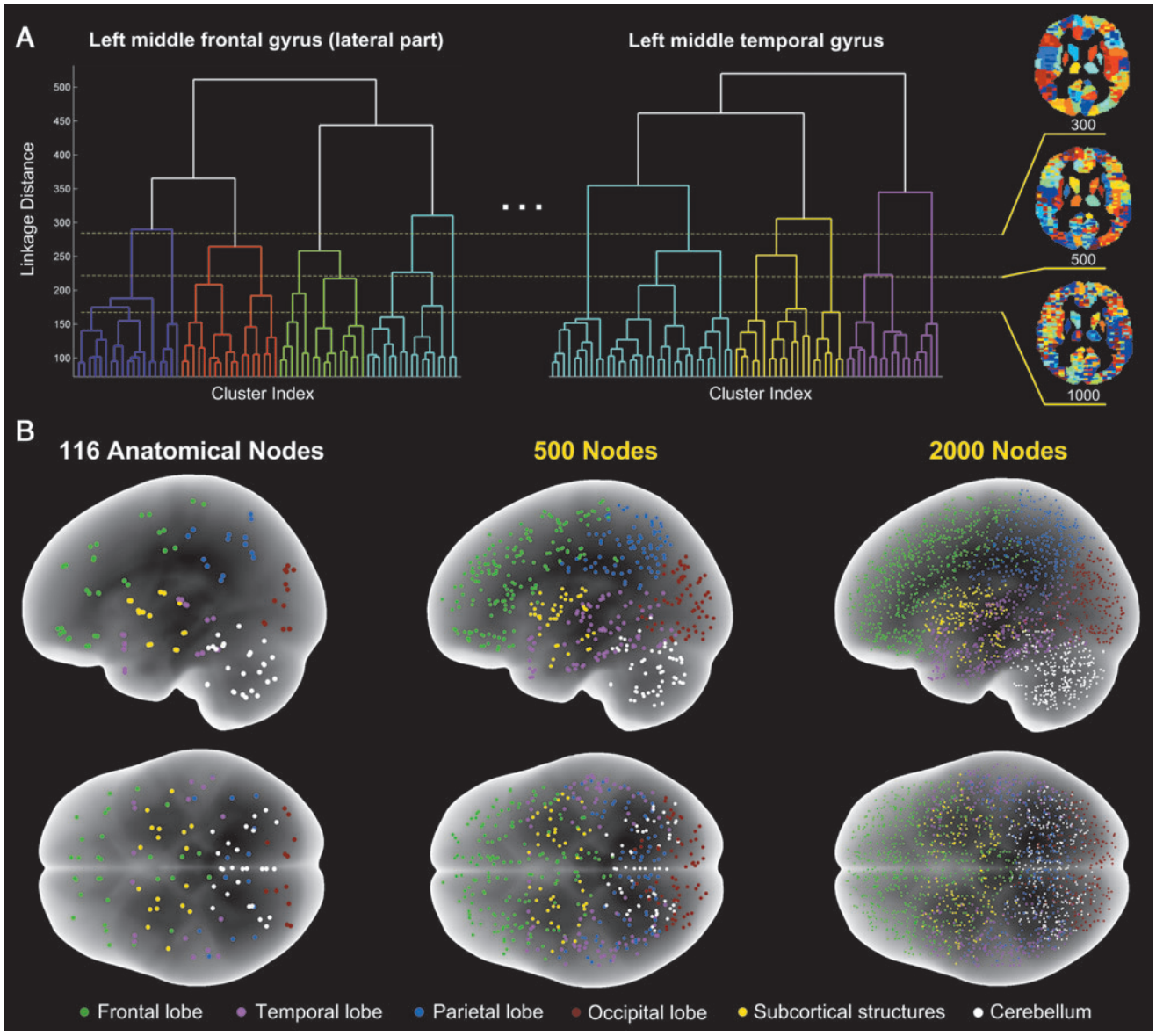

FIG. 1. Illustration of the anatomical-functional brain parcellation. **(A)** A combination of regional hierarchical clustering and global thresholding of dendrograms determines the spatial granularity of parcellation as shown for 300, 500, and 2000 nodes. **(B)** Glass-brain images of 116 anatomical regions (Tzourio-Mazoyer et al., 2002) and functional parcellations at 500 and 2000 nodes. Nodes in six major anatomical divisions are color coded. The plots are from one participant as an example.

transient effects in data acquisition. Subsequent data preprocessing included slice timing correction (*3dTshift* in AFNI), despiking (*3dDespike* in AFNI), and motion correction (*mcflirt* in FSL, producing three translational and three rotational parameters for each volume image). No significant differences of head motion in displacement and rotation were found between the four functional scan conditions, and the absolute mean displacement and rotation remained within a small range of values in all cases (wakefulness: mean displacement 0.21 ± 0.14 mm, mean rotation 0.26 ± 0.26^{o}; light sedation: 0.23 ± 0.20 mm, 0.26 ± 0.32^{o}; deep sedation: 0.31 ± 0.56 mm, 0.34 ± 0.54^{o}; recovery: 0.28 ± 0.25 mm, 0.3 ± 0.25^{o}). Physiological noise was estimated by using the average BOLD fMRI signals from regions of white matter (WM) and cerebrospinal fluid (CSF) determined in each individual's anatomical images. The voxel-wise BOLD fMRI signals from each run were then analyzed with a general linear regression model (*3dDeconvolve* in AFNI) by using the eight nuisance regressors representing noise artifacts from the motion variables (i.e., the three translational and three rotational motion time series), WM, and CSF, respectively. The residual signals of the regression analysis were considered representative of the denoised voxel-wise BOLD time series. We then applied a bandpass filter within 0.01–0.1 Hz to preserve only the low-frequency fluctuations in voxel-wise BOLD signals. To double check the effect of artifact suppression, additional analyses (not reported here) were conducted by using seed-based and ICA-based methods to evaluate the well-documented intrinsic connectivity networks of the brain, such as the default mode, executive control, and salience networks. All intrinsic brain networks can be identified clearly in consistency with prior studies

(Raichle, 2011). We also examined in each subject functional connectivity matrices among 116 anatomical regions of interest (ROIs) (Tzourio-Mazoyer et al., 2002) that cover the whole brain. No abnormal motion-induced global increases of functional connectivity among the ROIs were identified. Each participant's high-resolution anatomical images were then transformed to the standard MNI (Montreal Neuroimaging Institute) space (MNI152; *flirt* in FSL), followed by registering functional data (*flirt* in FSL) to the MNI space with a resampling to a 3-mm cubic voxel size.

Combined anatomical-functional network node parcellation scheme

The combined anatomical-functional parcellation defines an individual node as a cluster of voxels that shares a similar hemodynamic BOLD response profile at wakeful baseline but is constrained by the boundaries of a single anatomical structure (Liu et al., 2014). The parcellation consists of three steps (Fig. 1). First, 116 anatomical structures defined by a standard brain atlas (Tzourio-Mazoyer et al., 2002) were delineated in each participant's anatomical images in the MNI space. Second, hierarchical clustering was performed with the standardized BOLD time series of all voxels in each of the 116 anatomical structures separately. The hierarchical clustering resulted in 116 dendrograms based on computing the inner squared distances between voxel time series after normalization to z-scores. Third, a global cut-off threshold was applied to all 116 dendrograms to determine the number of clusters formed within each of the 116 anatomical structures and, therefore, the total number of nodes (Fig. 1A). The magnitude of this global threshold could be set flexibly at a desired spatial scale or granularity, at which a specific number of clusters (nodes) covering the whole brain were obtained (Fig. 1B). The mean BOLD time series of all voxels in each node was used to represent the node time series. Pearson cross-correlation between each node pair was computed, resulting in a symmetric matrix for each state of consciousness. Next, cross-correlation matrices of all participants were aligned to reference three-dimensional node coordinates from a representative participant based on a nearest-neighbor node-to-node alignment principle. In this way, a statistical comparison of paired group *t*-tests could be performed. We chose to construct brain networks at an increasing parcellation granularity, ranging from 116 anatomical nodes up to 2000 nodes.

State classification based on indices of decreased connectivity index and increased connectivity index

For state classification, we first identified node pairs that showed significant changes (increase and decrease) of the correlation coefficient (CC) by contrasting wakefulness and deep sedation by using a paired group *t*-test at a threshold of $p = 3.0 \times 10^{-5}$ at the brain parcellation of 2000 nodes. The *p*-threshold was chosen to aid the visual display of node pairs with significant connectivity changes without an excessive crowding of overlapping lines. The *p*-threshold was not corrected for multiple comparisons. Bonferroni correction for multiple comparisons would require $p \approx 2.5 \times 10^{-8}$, at which no node pair would survive. Therefore, we do not claim that a particular node pair is statistically significant in its association with alterations of consciousness. Instead, the choice of *p*-threshold served to define a suitable collection of node pairs that were used to differentiate a conscious state (wakeful baseline) from an unconscious state (deep sedation). As would be observed later, the choice of *p*-threshold did not influence the results and conclusions of our analysis.

With the collection of node pairs showing either increased or decreased functional connectivity between wakefulness and deep sedation, we defined two indices, the decreased connectivity index (DCI) and the increased connectivity index (ICI). In each of the four states of consciousness, the DCI was computed as the mean of the CCs of the collection of node pairs whose functional connectivity strength decreased in deep sedation relative to wakeful baseline. Likewise, the ICI was computed in each state as the mean of the CCs of the collection of node pairs whose functional connectivity strength increased in deep sedation relative to the wakeful baseline. We chose the contrast between wakefulness and deep sedation to select the node pairs for the calculation of DCI and ICI because they represented the two extreme states of consciousness in our experiment. We would then determine DCI and ICI for the other two states (light sedation and recovery) that presumably had intermediate values for the selected node pair groups.

The DCI and ICI from all study participants were plotted in a two-dimensional feature space. The performance of DCI and ICI to differentiate the four states of consciousness in individual participants was analyzed by quadratic discriminant analysis and leave-one-out cross-validation test. The choice of classifiers may be flexible. We chose a quadratic discriminant classifier (*classify* in Matlab) because it permits unequal class covariances, which is the case in our results. Leave-one-out cross-validation was used because of its relatively small sample size (15) in this study. Receiver operating characteristic (ROC) curves were computed for each step increase of the granularity of parcellation (ranging from 116 anatomical nodes to 2000 nodes) by adjusting the separating boundaries between two classes through varying the prior probability (the *prior* parameter of Matlab *classify* function) from 0 to 1. For parcellations at a smaller number of nodes, the *p*-threshold was chosen to generate approximately the same number of node pairs used for computing the DCI and ICI as those identified for brain parcellation at 2000 nodes. We quantified the overall classification performance by using the measure of area under the ROC curve (AUC).

Results

Propofol induced widespread functional connectivity changes during both light and deep sedation at $p = 3.0 \times 10^{-5}$ (Fig. 2A–G). Compared with wakeful baseline, the number of node pairs with reduced functional connectivity increased from light sedation (Fig. 2A) to deep sedation (Fig. 2B, C). Recovery showed a greater number of node connections with increased connectivity relative to deep sedation (Fig. 2D) than light sedation (Fig. 2B) and wakefulness (Fig. 2C). In comparison to wakeful baseline, light sedation, and recovery, deep sedation was also accompanied by increased functional connectivity, as indicated by the blue lines in Figure 2E–G, respectively. Overall, the extent of the changes of node connections showed a trend of scaling with the extent to which consciousness was modified. The number of node connections with increased and decreased functional connectivity for the seven comparisons are presented in Figure 2H at

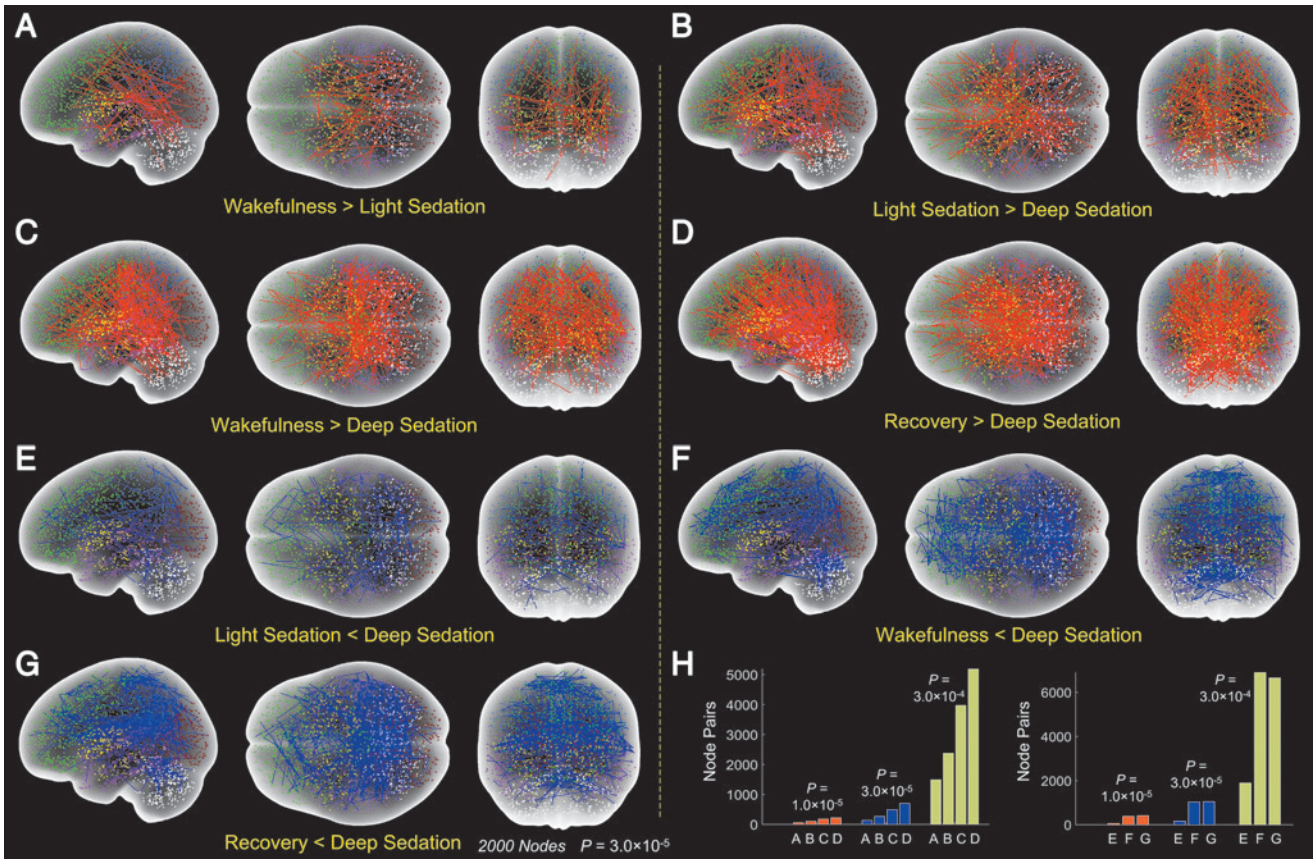

FIG. 2. Functional connectivity changes between various states of consciousness. **(A–G)** Seven state comparisons from group paired *t*-test at $p = 3.0 \times 10^{-5}$ with panels showing decreased node functional connectivity with deepening of sedation (red lines, **A–D)** and increased connectivity in deep sedation (blue lines, **E–G)**. The contrasts between wakefulness and deep sedation **(C** and **F)** were used to determine the collections of node pairs for computing DCI and ICI. Different dot colors distinguish major brain divisions, as indicated in Figure 1. **(H)** The number of connections at three different *p*-thresholds for the seven comparisons corresponding to panels **(A–G)**. The trend of changes in the number of node pairs is similar at the three *p*-thresholds. DCI, decreased connectivity index; ICI, increased connectivity index.

three different *p*-thresholds of 1.0×10^{-5}, 3.0×10^{-5}, and 3.0×10^{-4}. In spite of the different absolute number of node pairs at the different *p*-thresholds, the trends were very similar, suggesting that the choice of *p*-threshold was not critical. The distribution of node pairs with changing connectivity in six major anatomical divisions for various state comparisons is summarized in Table 1. The data suggest a prominent involvement of the frontal lobe, which is significantly greater than the other divisions ($p = 10^{-5}$, repeated-measures analysis of variance and Tukey-Kramer test of data from six independent state comparisons).

Distributions of the DCI and ICI in the two-dimensional feature space are shown for four selected parcellations in Figure 3A–D with 116, 300, 500, and 2000 nodes, respectively. With the most coarse-grained anatomical parcellation at 116 nodes, there was a substantial overlap among the

TABLE 1. PERCENTAGE DISTRIBUTION OF NODE PAIRS WITH ALTERED FUNCTIONAL CONNECTIVITY DEFINED AT $P = 3 \times 10^{-5}$ (GROUP PAIRED *T*-TEST) IN SIX MAJOR ANATOMICAL DIVISIONS

	Frontal	*Temporal*	*Parietal*	*Occipital*	*Subcortical*	*Cerebellar*
W>L	49	35	26	34	23	23
W<L	60	21	21	10	14	24
L>D	65	40	28	18	15	23
L<D	43	34	32	18	9	22
W>D	61	55	28	16	16	20
W<D	44	14	29	11	8	25
R>D	57	22	29	15	17	55
R<D	42	25	50	17	8	13

Symbols > and < indicate the comparison between states. The frontal lobe is affected more than any other region in all but one comparison. D, deep sedation; L, light sedation; R, recovery; W, wakefulness.

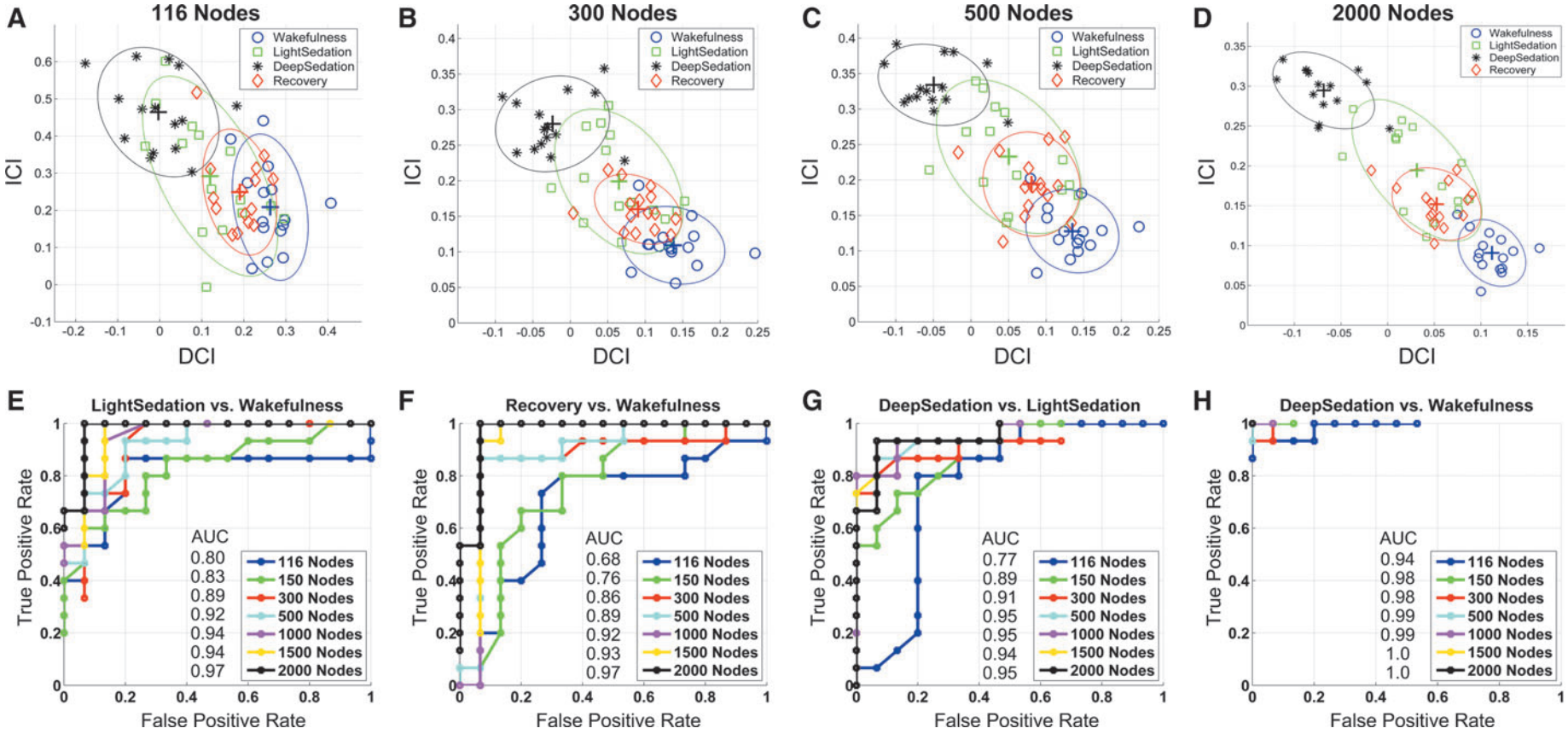

FIG. 3. ROC curve analysis of state classification. **(A–D)** Distribution of feature vectors defined by the DCI and ICI in the two-dimensional feature space. Color-coded symbols of feature vectors represent the four states of consciousness in all individual participants at the parcellation of 116, 300, 500, and 2000 nodes, respectively. The color-coded ellipses depict a two-dimensional Gaussian fitting of spatial distribution of feature vectors in each state. **(E–H)** The ROC curves describing true-positive versus false-positive rates by a quadratic discriminant analysis and leave-one-out cross-validation tests at increasing parcellation granularity in four conditions. AUC scores are shown for each parcellation. State classification in individual participants is distinctly better at 2000-node parcellation. AUC, area under curve; ROC, receiver operating characteristic.

feature vectors (defined by [DCI, ICI]) of the four states of consciousness. The feature vector cluster of wakefulness was well separated from that of deep sedation. However, the feature vector clusters of light sedation and recovery failed to separate from those of wakefulness and deep sedation or from each other at the 116-node parcellation. With an increase in the granularity of parcellation to 300, 500, and 2000, both between-cluster separation and within-cluster aggregation increasingly improved (Fig. 3B–D). In half of the participants, an overlap between light sedation and recovery remained even at the highest parcellation granularity, presumably due to an incomplete recovery from propofol sedation at the time of testing because of lingering effects of propofol, consistent with the results shown in Figure 2C.

The distribution of feature vectors at different parcellations resulted in consistent classification of the four states of consciousness (Fig. 3E–H). On comparing light sedation versus wakefulness, recovery versus wakefulness, and deep sedation versus light sedation, the ROC curves showed that parcellation at a higher granularity, especially at 2000 nodes, produced a superior classification, compared with the 116 anatomical parcellation (Fig. 3E–G). The AUC scores were 0.8, 0.68, and 0.77 for the 116-anatomical-node parcellation and 0.98, 0.97, and 0.95 for the 2000-node parcellation in Figure 3E–G, respectively, representing a 21% increase on average. Taken together, the results suggest that a fine-grained network parcellation provides a better separation of state-defining feature vectors and, therefore, a better overall classification of the states of consciousness led by anesthetic sedation in individual participants.

Discussion

We evaluated the benefit of defining functionally connected brain networks by using fine-grained anatomical-functional parcellation for the differentiation of states of consciousness as altered by graded propofol sedation. The extent of the changes of node connections showed a trend of scaling with the extent to which consciousness was altered. Previous studies suggested that brain parcellation at a higher than conventional granularity may provide a better delineation of topological and connectional features of the brain (Hayasaka and Laurienti, 2010; Liu et al., 2014; Zalesky et al., 2010). Consistent with our anticipation, we found that parcellation at a higher granularity at or approaching 2000 nodes enabled a better differentiation of the states of consciousness in individual participants than what could be obtained at a coarse-grained parcellation using 116 anatomically defined brain regions. Whether such a finding can be generalized to other quantitative measures of connectivity and/or BOLD fMRI signals needs to be further investigated.

The improvement in classification performance at a fine-grained network parcellation is most likely due to the capacity of the parcellation algorithm that combines the anatomical and functional features of each identified brain subdivision or parcel. As we know, macroscopic anatomical boundaries have a general, though imperfect, relation to functional boundaries. The proposition of a nested network organization in the central nervous system suggests that the basic functional units of the brain first emerge individually within each of the individual anatomical structures (Agnati et al., 2004). Thus, defining the network nodes as clusters of anatomically constrained voxels that share similar correlated BOLD fluctuations leads to increased node functional specificity, compared with that at coarse-grained anatomical parcellations (Fischl et al., 2004), and reduced noise influence and node redundancy, as compared with the voxel-based approach (Eguiluz et al., 2005; van den Heuvel et al., 2008). It is likely that there might exist an optimal spatial scale that would allow the best characterization of topological features and network organizations of the brain in individual applications (Hayasaka and Laurienti, 2010; Zalesky et al., 2010). Therefore, our brain parcellation approach represents a useful extension to the existing brain parcellation methods in the literature (de Reus and van den Heuvel, 2013).

Another advantage of our parcellation approach is that it is easy to use. Unlike other approaches for determining areal maps of the brain based on multimodal imaging techniques and complicated machine-learning algorithms (Glasser et al., 2016), it requires no additional data acquisition of different imaging modalities other than BOLD fMRI and T1-contrast-based anatomical images, which are commonly available in nearly all reported fMRI studies. Thus, our approach can be readily extended to many available data sets. In addition, the parcellation approach offers full flexibility to examine the brain as a connected network at an arbitrary spatial granularity (i.e., via adjusting the global cut-off threshold), while keeping a consistent principle in defining the anatomical and functional significances of each identified parcel (or node). Meanwhile, it provides an individual-subject-based brain parcellation scheme, offering opportunities for an individual analysis of functional reorganization within or across specific anatomical regions (e.g., changes in the number of functionally distinct subdivisions/parcels in one or more anatomical/functional systems across different brain states).

Alterations in the state of consciousness during anesthesia and sedation have been linked to selective changes in functional and effective connectivity in the brain (Alkire, 2008; Alkire et al., 2008; Demertzi et al., 2013; Hudetz, 2012; Langsjo et al., 2014; Nallasamy and Tsao, 2011). In the present investigation, we examined long-range connectivity among relatively large brain regions (four cortical lobes, subcortex, and cerebellum), which was a convenient and theory-inspired choice to evaluate the effect of parcellation on differentiating four states of consciousness. At the chosen p-threshold, we found a significant difference in the relative involvement of six major anatomical divisions in node connectivity changes across the states of consciousness. In particular, the frontal lobe had the most prominent and consistent involvement in node connectivity changes when contrasting the various conditions. The key importance of the frontal lobe has been postulated in various theories of consciousness. Both the global workspace theory (Baars, 2002, 2005) and the related global neuronal workspace model (Dehaene et al., 2003) emphasize the roles of the frontal lobe in generating conscious perception. Prior studies have also highlighted a preferential suppressive effect of propofol on activity and connectivity of the frontal lobes (Boveroux et al., 2010; Guldenmund et al., 2016; Liu et al., 2016) and in other cases with the use of sevoflurane (Deshpande et al., 2010; Palanca et al., 2015). A new finding of this study is that both the increase and the decrease of functional connectivity during deep sedation have the strongest association with the frontal lobe, suggesting that various subregions of the frontal lobe may be associated with differential, possibly competing roles in maintaining conscious

activities during wakeful baseline and perhaps operating on internally generated neuronal processes during deep sedation.

In addition to long-range connectivity, local connectivity changes may also be linked to different states of consciousness. Previous investigations suggested the importance of both within- and between-network connectivity in anesthetic-induced unconsciousness (Boveroux et al., 2010; Deshpande et al., 2010; Kafashan et al., 2016). Our parcellation methodology should lend itself to the investigation of intra-network connectivity. Future investigations could also focus on the connectivity of smaller regions, potentially all the way down to the voxel level.

It may also be of interest to apply our new parcellation method to neurological patients with brain injuries. However, with severely deformed brains, the automated anatomical partitioning may be problematic, in which case one may resort to relying mainly on functional parcellation, skipping the anatomical parcellation step, or using a simplified anatomical parcellation, for example, keeping only manual or automated delineations of lobe boundaries. This approach may be tested in future. A limitation of this study is that the sample size (15) is relatively small, and we had to adopt a leave-one-out cross-validation approach for the evaluation of the classifier's performance. Thus, the nature of classifications should be considered as more descriptive than predictive. Nevertheless, what should be emphasized is the evident increase of separation among feature clusters of the four states of consciousness with the increase of spatial granularity (Fig. 3A–D). The choice of classifiers, however, is flexible (e.g., discriminant analysis or artificial neural network models).

In summary, our study proposed a BOLD fMRI-based approach for defining brain networks at a high spatial granularity. The preliminary results suggest that it may provide a superior imaging-based distinction of the graded effect of anesthesia on consciousness. Despite the technical issues existing in overcoming the problem of correction for multiple comparisons when fine-grained areal maps of the entire brain are considered, our combined functional-anatomical parcellation approach provides a principled way and a useful extension to the current literature in evaluating brain functions at a high spatial granularity.

Acknowledgments

The research reported in this publication was supported by grants from the National Institute of General Medical Sciences of the National Institutes of Health under Award Number R01 GM103894 and T32 GM89586. The content is solely the responsibility of the authors and does not necessarily represent the official views of the National Institutes of Health. The authors thank Ms. Lydia Washechek, BA, for editorial assistance.

Author Disclosure Statement

No competing financial interests exist.

References

Agnati LF, Santarossa L, Genedani S, Canela EI, Leo G, Franco R, et al. 2004. On the nested hierarchical organization of CNS: basic characteristics of neuronal molecular organization. Cortical Dynamics LNCS 3146. Erdi P., Springer, Berlin:24–54.

Alkire MT. 2008. Loss of effective connectivity during general anesthesia. Int Anesthesiol Clin 46:55–73.

Alkire MT, Hudetz AG, Tononi G. 2008. Consciousness and anesthesia. Science 322:876–880.

Baars BJ. 2002. The conscious access hypothesis: origins and recent evidence. Trends Cogn Sci 6:47–52.

Baars BJ. 2005. Global workspace theory of consciousness: toward a cognitive neuroscience of human experience. Prog Brain Res 150:45–53.

Boveroux P, Vanhaudenhuyse A, Bruno MA, Noirhomme Q, Lauwick S, Luxen A, et al. 2010. Breakdown of within- and between-network resting state functional magnetic resonance imaging connectivity during propofol-induced loss of consciousness. Anesthesiology 113:1038–1053.

Chalmers DJ. 1998. The problems of consciousness. Adv Neurol 77:7–16.

de Reus MA, van den Heuvel MP. 2013. The parcellation-based connectome: limitations and extensions. Neuroimage 80:397–404.

Dehaene S, Sergent C, Changeux JP. 2003. A neuronal network model linking subjective reports and objective physiological data during conscious perception. Proc Natl Acad Sci U S A 100:8520–8525.

Demertzi A, Soddu A, Laureys S. 2013. Consciousness supporting networks. Curr Opin Neurobiol 23:239–244.

Deshpande G, Kerssens C, Sebel PS, Hu X. 2010. Altered local coherence in the default mode network due to sevoflurane anesthesia. Brain Res 1318:110–121.

Eguiluz VM, Chialvo DR, Cecchi GA, Baliki M, Apkarian AV. 2005. Scale-free brain functional networks. Phys Rev Lett 94:018102.

Fischl B, van der Kouwe A, Destrieux C, Halgren E, Segonne F, Salat DH, et al. 2004. Automatically parcellating the human cerebral cortex. Cereb Cortex 14:11–22.

Glasser MF, Coalson TS, Robinson EC, Hacker CD, Harwell J, Yacoub E, et al. 2016. A multi-modal parcellation of human cerebral cortex. Nature 536:171–181.

Godwin D, Barry RL, Marois R. 2015. Breakdown of the brain's functional network modularity with awareness. Proc Natl Acad Sci U S A 112:3799–3804.

Guldenmund P, Gantner IS, Baquero K, Das T, Demertzi A, Boveroux P, et al. 2016. Propofol-induced frontal cortex disconnection: a study of resting-state networks, total brain connectivity, and mean BOLD signal oscillation frequencies. Brain Connect 6:225–237.

Hayasaka S, Laurienti PJ. 2010. Comparison of characteristics between region-and voxel-based network analyses in resting-state fMRI data. Neuroimage 50:499–508.

Huang Z, Zhang J, Wu J, Qin P, Wu X, Wang Z, et al. 2016. Decoupled temporal variability and signal synchronization of spontaneous brain activity in loss of consciousness: an fMRI study in anesthesia. Neuroimage 124:693–703.

Hudetz AG. 2012. General anesthesia and human brain connectivity. Brain Connect 2:291–302.

Kafashan M, Ching S, Palanca BJ. 2016. Sevoflurane alters spatiotemporal functional connectivity motifs that link resting-state networks during wakefulness. Front Neural Circuits 10:107.

Langsjo JW, Revonsuo A, Scheinin H. 2014. Harnessing anesthesia and brain imaging for the study of human consciousness. Curr Pharm Des 20:4211–4224.

Liu X, Lauer KK, Douglas Ward B, Roberts C, Liu S, Gollapudy S, et al. 2016. Propofol attenuates low-frequency fluctuations of resting-state fMRI BOLD signal in the anterior frontal cortex upon loss of consciousness. Neuroimage 147:295–301.

Liu X, Ward BD, Binder JR, Li SJ, Hudetz AG. 2014. Scale-free functional connectivity of the brain is maintained in anesthetized healthy participants but not in patients with unresponsive wakefulness syndrome. PLoS One 9:e92182.

Martuzzi R, Ramani R, Qiu M, Rajeevan N, Constable RT. 2010. Functional connectivity and alterations in baseline brain state in humans. Neuroimage 49:823–834.

Mashour GA. 2013. Cognitive unbinding: a neuroscientific paradigm of general anesthesia and related states of unconsciousness. Neurosci Biobehav Rev 37:2751–2759.

Monti MM, Lutkenhoff ES, Rubinov M, Boveroux P, Vanhaudenhuyse A, Gosseries O, et al. 2013. Dynamic change of global and local information processing in propofol-induced loss and recovery of consciousness. PLoS Comput Biol 9:e1003271.

Monti MM, Vanhaudenhuyse A, Coleman MR, Boly M, Pickard JD, Tshibanda L, et al. 2010. Willful modulation of brain activity in disorders of consciousness. N Engl J Med 362:579–589.

Nallasamy N, Tsao DY. 2011. Functional connectivity in the brain: effects of anesthesia. Neuroscientist 17:94–106.

Palanca BJ, Mitra A, Larson-Prior L, Snyder AZ, Avidan MS, Raichle ME. 2015. Resting-state functional magnetic resonance imaging correlates of sevoflurane-induced unconsciousness. Anesthesiology 123:346–356.

Power JD, Cohen AL, Nelson SM, Wig GS, Barnes KA, Church JA, et al. 2011. Functional network organization of the human brain. Neuron 72:665–678.

Raichle ME. 2011. The restless brain. Brain connect 1:3–12.

Scheinost D, Benjamin J, Lacadie CM, Vohr B, Schneider KC, Ment LR, et al. 2012. The intrinsic connectivity distribution: a novel contrast measure reflecting voxel level functional connectivity. Neuroimage 62:1510–1519.

Schroter MS, Spoormaker VI, Schorer A, Wohlschlager A, Czisch M, Kochs EF, et al. 2012. Spatiotemporal reconfiguration of large-scale brain functional networks during propofol-induced loss of consciousness. J Neurosci 32:12832–12840.

Schrouff J, Perlbarg V, Boly M, Marrelec G, Boveroux P, Vanhaudenhuyse A, et al. 2011. Brain functional integration decreases during propofol-induced loss of consciousness. Neuroimage 57:198–205.

Shafer A, Doze VA, Shafer SL, White PF. 1988. Pharmacokinetics and pharmacodynamics of propofol infusions during general anesthesia. Anesthesiology 69:348–356.

Tagliazucchi E, Chialvo DR, Siniatchkin M, Amico E, Brichant JF, Bonhomme V, et al. 2016. Large-scale signatures of unconsciousness are consistent with a departure from critical dynamics. J R Soc Interface 13:20151027.

Tononi G. 2012. Integrated information theory of consciousness: an updated account. Arch Ital Biol 150:293–329.

Tzourio-Mazoyer N, Landeau B, Papathanassiou D, Crivello F, Etard O, Delcroix N, et al. 2002. Automated anatomical labeling of activations in SPM using a macroscopic anatomical parcellation of the MNI MRI single-subject brain. Neuroimage 15:273–289.

van den Heuvel MP, Sporns O. 2011. Rich-club organization of the human connectome. J Neurosci 31:15775–15786.

van den Heuvel MP, Stam CJ, Boersma M, Hulshoff Pol HE. 2008. Small-world and scale-free organization of voxel-based resting-state functional connectivity in the human brain. Neuroimage 43:528–539.

Zalesky A, Fornito A, Harding IH, Cocchi L, Yucel M, Pantelis C, et al. 2010. Whole-brain anatomical networks: does the choice of nodes matter? Neuroimage 50:970–983.

Address correspondence to:
Xiaolin Liu
Department of Radiology
Center for Imaging Research
Medical College of Wisconsin
8701 Watertown Plank Road
Milwaukee, WI 53226

E-mail: xiliu@mcw.edu

Anthony G. Hudetz
Department of Anesthesiology
Center for Consciousness Science
University of Michigan
1301 East Catherine Street
Ann Arbor, MI 48109

E-mail: ahudetz@med.umich.edu